Bioinspiration &
Biomimetics

PAPER • **OPEN ACCESS**

Nodes for modes: Nodal honeycomb metamaterial enables a soft robot with multimodal locomotion

To cite this article: Yusuf Dikici *et al* 2024 *Bioinspir. Biomim.* **19** 046002

IOP Publishing Bioinspir. Biomim. 19 (2024) 046002 https://doi.org/10.1088/1748-3190/ad3ff8

Bioinspiration & Biomimetics

OPEN ACCESS

RECEIVED
5 February 2024

REVISED
31 March 2024

ACCEPTED FOR PUBLICATION
17 April 2024

PUBLISHED
7 May 2024

PAPER

Nodes for modes: Nodal honeycomb metamaterial enables a soft robot with multimodal locomotion

Yusuf Dikici[1,4], **Kathryn Daltorio**[1,*] and **Ozan Akkus**[1,2,3,*]

[1] Department of Mechanical and Aerospace Engineering, Case Western Reserve University, Cleveland, OH, United States of America
[2] Department of Biomedical Engineering, Case Western Reserve University, Cleveland, OH, United States of America
[3] Department of Orthopedic Surgery, University Hospitals Cleveland Medical Center, Cleveland, OH, United States of America
[4] Department of Mechanical Engineering, Bartın University, Bartın, Turkey
[*] Authors to whom any correspondence should be addressed.

E-mail: kati@case.edu, oxa@case.edu and yusuf@case.edu

Keywords: soft robot, metamaterial, multimodal locomotion, limbless locomotion

Supplementary material for this article is available online

Abstract

Soft-bodied animals, such as worms and snakes, use many muscles in different ways to traverse unstructured environments and inspire tools for accessing confined spaces. They demonstrate versatility of locomotion which is essential for adaptation to changing terrain conditions. However, replicating such versatility in untethered soft-bodied robots with multimodal locomotion capabilities have been challenging due to complex fabrication processes and limitations of soft body structures to accommodate hardware such as actuators, batteries and circuit boards. Here, we present MetaCrawler, a 3D printed metamaterial soft robot designed for multimodal and omnidirectional locomotion. Our design approach facilitated an easy fabrication process through a discrete assembly of a modular nodal honeycomb lattice with soft and hard components. A crucial benefit of the nodal honeycomb architecture is the ability of its hard components, nodes, to accommodate a distributed actuation system, comprising servomotors, control circuits, and batteries. Enabled by this distributed actuation, MetaCrawler achieves five locomotion modes: peristalsis, sidewinding, sideways translation, turn-in-place, and anguilliform. Demonstrations showcase MetaCrawler's adaptability in confined channel navigation, vertical traversing, and maze exploration. This soft robotic system holds the potential to offer easy-to-fabricate and accessible solutions for multimodal locomotion in applications such as search and rescue, pipeline inspection, and space missions.

1. Introduction

Animals like worms and snakes are able to use their soft bodies to locomote in various modes to traverse a wide variety of environmental situations on land and water. Without legs, wheels or tracks, they create paths in heterogeneous piles of rock and debris, climb over roots, and squeeze into narrow burrows. Limbless animals have multiple muscles that are distributed along the body [1–3]. High degrees of freedom (DoF) in actuation, combined with the softness of the animals' body, enables the performance of versatile locomotion modes, equivalent to different walking gaits for different environments. In soft robotics, mimicking these behaviors is essential for accessing otherwise inaccessible confined spaces [4–6]. While we and others have demonstrated soft bodied locomotion, past iterations were generally limited in terms of the DoF of actuation and number of actuator, limiting the multimodality of locomotions [7, 8]. Also, operation in unstructured environment as a target application requires the robot body to accomodate on-board power and control hardware in an untethered fashion. Achieving multimodality in soft-body locomotion arises from the challenges of fabricating a soft body and attaching many electronic components (which are typically hard) to the body structure (which is typically soft to enable passive compliance). Therefore, simplicity of fabrication and attainment of hardware integration

may extend the capabilites of soft-bodied robots and bridge the gap to their applicability in real-world applications [9].

Soft robots are conventionally fabricated with materials that are inherently soft. The use of such materials enables these robots to conform to the environment. However, a limitation of fully soft robots is their dependence on external actuation and power sources, such as pneumatic pumps and batteries, thereby necessitating tethered connections that may limit operational range. In contrast, the incorporation of rigid elements within soft robot structures has proven beneficial for achieving autonomy in these systems [10, 11]. These robots, categorized as 'Employs Soft Matter' in on ontological classification of soft robots [12], facilitates the integration of actuators and electronic devices within the robot's structure, without compromising its compliance. Similar approaches may be followed to integrate sufficient number of actuators which is required for versatile locomotion modes.

One mode, peristaltic locomotion, is valuable for operation in confined spaces by squizing segments which is achieved with soft actuators and soft segments. Typically, perisaltic robots are designed with multiple segments, each of which contains actuators that elongate or contract sequentially [1]. For example, commonly used extensional pneumatic actuators generate segment elongation when pressurized [13–17]. Similarly, actuatable materials such as nitinol wires [18, 19] or polymers [20] respond to heat by contracting or bending. Each segment can have as many as two DoF if the robot can steer.

Undulatory locomotion modes (e.g. serpentine, sidewinding, anguilliform), which are essential for efficient omnidirectional locomotion in open areas, requires many segments and more bending at each segment. Most soft robots are thus designed for one primary mode of locomotion.

There have been successful attempts to integrate soft robots with multimodal locomotion capability. 3D soft robotic snake, of which segments consist of three extensional actuators, performs serpentine, sidewinding and step climbing [21]. Another example, the WSIM robot [22] which was designed with compliant worm segments, actuated with servomotors, is capable of peristalsis and undulation. Similarity of these examples is both designs depends on integrated (hard) wheels in snake locomotion. This dependance may be eliminated and locomotion may be generated solely via soft body movements with the integration of more and compact segments in the body structure.

In entirely soft robots, it is not easy to scale up the number of custom soft actuators per segment. Molding silicone tubes and placing fiber reinforcements for pneumatic actuators [13, 23], integrating nitinol wires in soft mesh [18, 24] and preparing resistor-integrated polymers [20] require complex and manual designs and fabrication processes. Furthermore, soft robots are typically tethered to a power source or a air/fluid pump through cables or tubing which limit the range of motion.

Fortunately, robotic electronic components have decreased in size in recent years such that they are small enough to be embedded in soft robots. Servomotors are typically the most robust and the easiest-to-use actuators in terms of cost, reliability, and physical simplicity and were utilized in previous studies [22, 25–27]. Servomotor control is possible using small sized microcontrollers and portable batteries that can be accommodated on board the robot [22]. Our previous studies successfully integrated servomotors with a compliant mesh body structure of earthworm robots [28–30]. Our design enabled studying sensor feedback [31], control of slip [32], and speed and cost of transport optimization [33]. Despite these achievements, the stiffness of the mesh structure limited the bending angle in segments as well as undulation. Consequently, we have been searching for body designs that provide a combination of high compliance and secure mounting points for electronic components such as servomotors. Because a 'confined space' can have different minimal passable diameters, we wanted a design that scales. Ease of fabrication is also an important factor. Thus, we approached the problem from a materials design perspective, leading to a metamaterial approach.

Mechanical metamaterials are engineered structures of which mechanical properties primarily originate from their unit cell geometries [34–36]. Various structural configurations have been developed to create mechanical metamaterials, such as lattice [37, 38], origami [39, 40], kirigami [41, 42], tensegrity [26], etc. to create unique programmable functions like high Poisson's ratio ($\nu > 0.5$), negative Poisson's ratio [43], deployability [44], negative compressibility [45], etc. For example, in our previous study, we reported an analytical model for nodal honeycomb lattice, characterizing Poisson's ratio and Young's modulus parameters, and demonstrated a mathematical procedure providing its physical and mechanical integration with auxetic anti-tetrachiral lattice to create custom, shape morphing, soft-bodied robots. With this and similar studies, lattice structures have reached the highest maturity level in the field [35]; however, they are underutilized in soft robotics—with a notable exception being hydrosnake [27], of which sections was injection molded and 'discretely assembled' [46] with rivet connections. Utilization of 3D printing would be more convenient

than molding for quick development, and may result in a robust multi-functional platform.

Here we present MetaCrawler, the first 3D printed metamaterial soft robot capable of multiple locomotion modes (peristalsis, sidewinding, sideways translation, turn-in-place and anguilliform). Our design enables a simple, semi-automated fabrication process to create the body structure with many compact segments. Thus, the robot can perform multiple soft body locomotion without relying on assisting hard-robotic components, like wheels. Enabled by a judicious design and facile assembly of hard and soft phases, servo actuators, batteries and electronic components are attached to the nodes in a nodal honeycomb lattice. As a result, the robot operates untethered. Another advantage is that the speed and passable dimensions for peristaltic locomotion are functions of the lattice parameters, suggesting that different designs can be printed for different environments. The robustness and scalability of this design enabled us to provide unique demonstrations, including swimming, retrieval of an object in a pipe, and traversal of various mazes by combining different modes. These demonstrations show the feasibility of adapting this platform for future uses in search and rescue, pipeline inspection or space missions in which a soft robot may need to be printed on demand.

2. Design and fabrication of compliant body structure

Our goal was to create an easy-to-fabricate soft body that integrates all the actuation components. The soft body needs to deform to enable the absolute value of the effective Poission's ratio to be large for peristaltic locomotion [33], while the actuators need secure attachment points with low local strain. The nodal honeycomb, which we previously reported [47], satisfies these design goals with deformable ligaments and stiff nodes (figure 1(a)).

We designed a tubular configuration of nodal honeycomb to mimic slender bodies of limbless animals. The structure was designed with octagonal cross-sectional profile to maintain in-plane deformation behavior of ligaments (figure 1(b)). To simplify the fabrication process and create compatible node design with servomotors, we modularized the nodal honeycomb structure into hard nodes and soft connectors (figure 1(c)). All components of modular nodal honeycomb structure were 3D printed with a commercial desktop 3D printer (Ultimaker S3, Ultimaker BV). Nodes as well as other rigid components used in MetaCrawler are fabricated with Polylactide filament (PLA, 3500 MPa) and connectors were 3D printed with Thermoplastic Polyurethane (TPU, 12 MPa). 3D printing process for all components took 96 h with a single 3D printer. Technical details of the 3D printing process is available in Supplementary Document.

Components were assembled by interlocking the slots on the nodes with the blocks on the ends of connectors via press-fit fastening (figure 1(e)). The robot presented in this study was built with 12 segments. Each segment of MetaCrawler body structure has 4 connectors and 4 nodes (48 connectors and 48 nodes in total). At the standing state of the robot, nodes in a segment are positioned as one on bottom, one on top and two on sides.

3. System integration and control architecture

The key to multimodal locomotion in MetaCrawler is including high DoF provided by independently actuated servomotors integrated in each segment, similar to the way animals engage multiple muscles. Hyper-redundant robots are typically considered difficult to make untethered because of limited space in the body structures. MetaCrawler's design overcame this obstacle by accomodating the electronic and actuation components distributed over the 48 nodes.

The nodes on the left and right sides of the body housed the servomotors and the spools to which tendon strings are attached (figure 2(a)). We choose 9 g metal geared micro servomotors (MG90S, ETMall) for their compact size. The servo horns and spools were placed on the motor shafts inside the nodes. Circumferentially-running are tendons (abrasion resistant monofilament nylon fishing lines) which are attached to the spools and connected to the top and bottom nodes (figure 2(b)). When the servomotors rotate the spools, the tendons are pulled, reducing the circumference of the segments on each side (figures 2(c) and (d)). To keep tension in the strings, the maximum segment diameter position is designed to have an initial bias of 10% contraction (figure 2(c)). The radius of spools is designed to provide maximum contraction (minimum diameter) when the servo angle reaches 180°. In other words, semicircumference of the spool (for servomotors with 180° rotation range) must be equal with the applied displacement range of connectors (figure 2(d), supplementary document).

Control circuits and batteries, of which circuit diagram shown in figure 2(e), are mounted on top and bottom nodes. Further details on these components are in the Supplementary Document. Assembling the complete robot as shown in figure 2(f) including body structure and system integration took approximately 1 h and 30 min. The fully assembled robot weighs 1.2 kg and measures 99.3 cm in length.

Different locomotion modes result from different sequences of actuation that travel down the

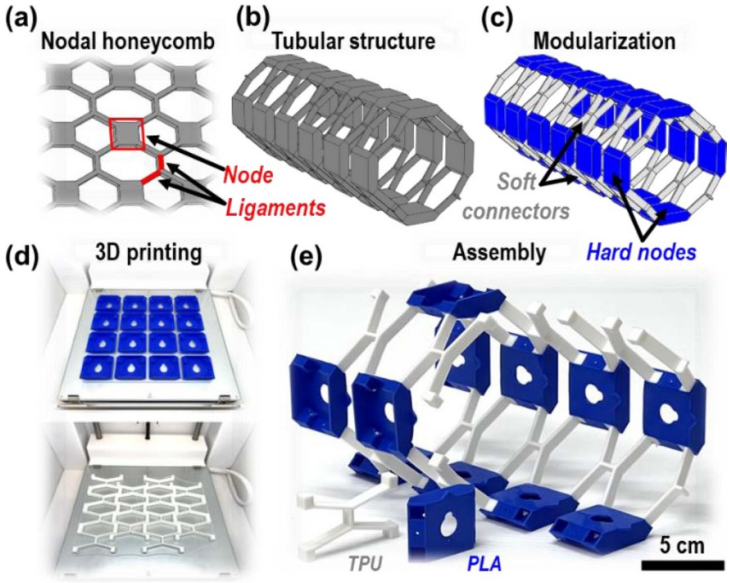

Figure 1. Design and fabrication of the compliant metamaterial body. (a) The design of MetaCrawler was inspired by the 2-dimensional nodal honeycomb cellular structure of which unit cells contains nodes and ligaments. (b) Tubular form of nodal honeycomb with an octagonal cross-section was used for body structure. (c) To simplify the design and fabrication, the structure was modularized into nodes and connectors. (d) Connectors provide compliance to the structure and nodes facilitate actuation and control components; therefore, nodes and connectors were 3D printed separately with hard and soft materials, respectively. The 3D printer used in this study is an Ultimaker S3 (Ultimaker BV). (e) Nodes and connectors were assembled with press-fit based attachment. The blocks on connector tips were connected in the slots on nodes. Dimensions of connectors and nodes are presented in figure 3(b).

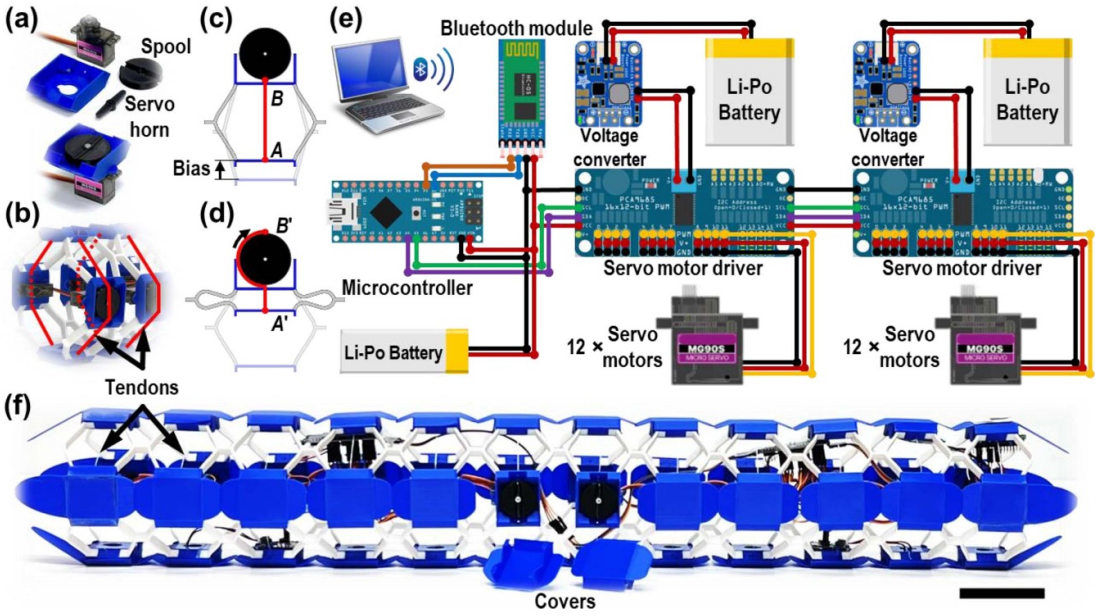

Figure 2. Actuation system integration on MetaCrawler. (a) Servo motors were placed on lateral nodes, and servo horns and spools were mounted on the shaft. (b) Spools were connected to the top and bottom nodes with tendons. (c) In order to maintain tension, tendons were placed applying a bias of 10% to connectors in expanded state of segments. (d) The diameter of spools was set to fully contract connectors when servo angle is 180°. (e) Electronic schematics as shown were distributed along the body of the robot and connecting wires were managed not to affect segment deformation. (f) After fully assembling the robot (sideview), exteriors of nodes were capped with covers. The scale bar represents a length of 5 cm.

left and right side of the robot's body. These actuation sequences are programmed in Arduino IDE (Arduino) as while-loops which repeat the wave propagation cycle until the operator at the computer stops the sequence or switches to another locomotion mode. Locomotion programs are encoded in the microcontroller and remotely controlled via Bluetooth communication (figure 2(f)). Libraries used in programming are provided in the supplementary document.

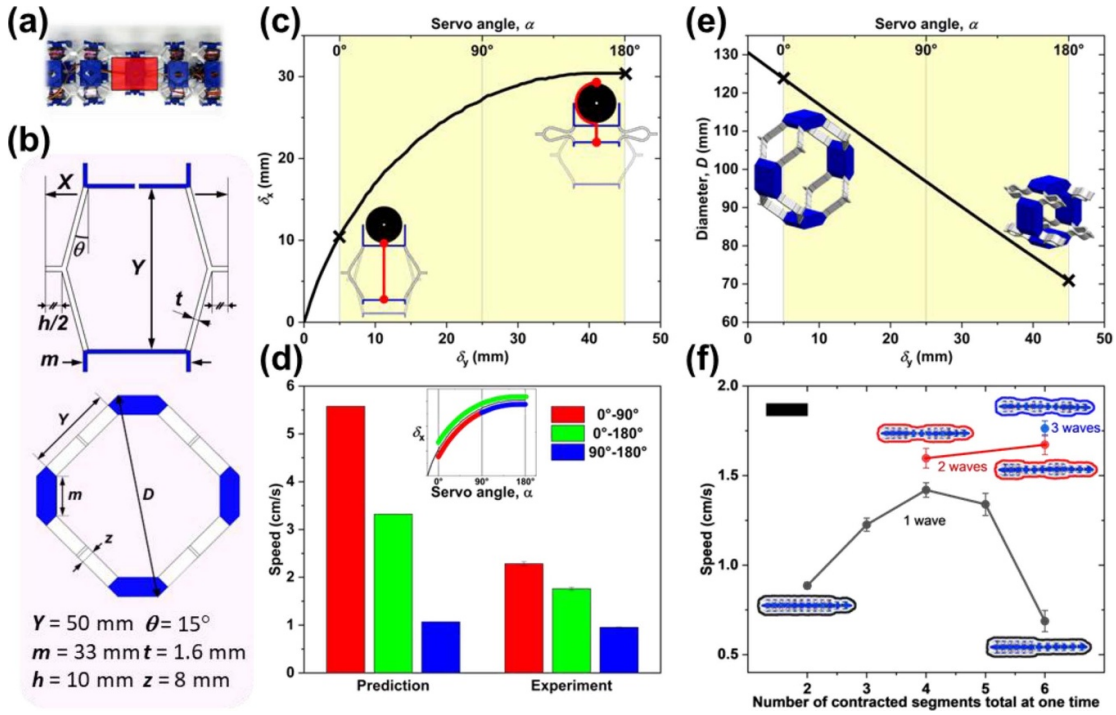

Figure 3. Analysis of segment contraction. (a) Segments consist of nodal honeycomb unit cells which horizontally elongate under applied vertical contraction. (b) Dimensions of geometrical features of unit cells and segments are demonstrated. Top: Front view of a unit cell. Bottom: Cross-section view of a segment. (c) Compression tests on connectors show that the perpendicular and lateral displacement of nodal honeycomb unit structure is non-linear. Yellow region on the plot is the deformation space which servomotor control and generate locomotion with. Because tendons are placed in such a way that they apply a bias of a 10% contraction on unit cells, yellow region starts from $\delta_y = 5$ mm. At $\delta_y = 45$ mm, unit cells are fully contracted. (d) Non-linear deformation on unit cells results in different robot speeds when different ranges of servomotor rotation are used. The velocities from analytical predictions were compared with experiments for three servomotor rotation ranges: 0°–90°, 0°–180° and 90°–180°. Specifically, using only the first half of range (0°–90°) results in more than doubling speed. (e) The diameter of a segment (D shown in (b)) at a specified applied displacement (δ_y) was analytically formulated (equation (S4)) and plotted to determine the effective servo angle at expanded state when traversing in confined channels, where speeds will need to be reduced. (f) Locomotion speeds with six different waveforms were compared. Increasing number of waves improves speed because the weight of contracted segments is distributed along the anchoring segments more evenly. Embedded images show top view of MetaCrawler. The scale bar represents a length of 50 cm.

4. Segment contraction: peristaltic locomotion

Peristaltic locomotion occurs when waves of contraction travel down the body. Synchronous actuation of the two servomotors in a given segment decreases in diameter of the segment while increasing the length (figure 3(a)). This length-diameter coupling underpins the peristaltic locomotion capability, both forward and backward [48]. Accordingly, we conducted compression tests of unit cells (figure 3(b)) to determine the relation between vertical contraction on unit cells, $\boldsymbol{\delta_y}$ (which leads the cirumferencial contraction), and the resulting lateral elongation, $\boldsymbol{\delta_x}$, (figure 3(c)) across the full range of servomotor angles (0°–180°). Methods associated with these mechanical tests on unit cells are detailed in the Supplementary Document. The decreasing slope of this line implies that the robot will move faster when the servomotor angles move between 0° and 90° rather than utilizing the full range of rotation. An analytical model is developed as detailed in the supplementary document (equations (S1)–(S3)) to predict the velocity of the robot as a function of unit cell elongation ($\boldsymbol{\delta_x}$), stroke time of servomotots ($\boldsymbol{T}$) and the number of segments ($\boldsymbol{S}$) and the number of contracted segments ($\boldsymbol{C}$).

We measured the velocity of the robot and compared these results with analytical predictions (figure 3(d)). Following the wave description conventions in previous studies [28, 33] (Actuation sequences of peristaltic locomotion modes are demonstrated in figure S2 and example codes used for programming locomotion are reported in supplementary document), the fastest velocity resulted from 2 × 3 peristalsis waveform (2 contracted segments per wave, and 3 waves along the body at any time) ($\boldsymbol{C} = 6$, $\boldsymbol{S} = 12$). As predicted, the robot was more than twice as fast when using the lower half of the range of motion only (0°–90°) than when using the upper half of the range of motion (90°–180°). Thus, on flat smooth ground, keeping the

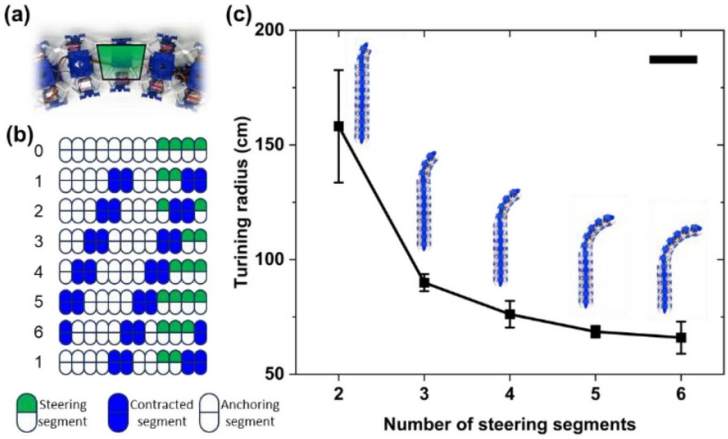

Figure 4. Segment flexure and steering. (a) Flexure in a segment: Asynchronous actuation (actuating one servomotor in a segment) results in flexure in a segment because segment elongates in only the actuated side. (b) Actuation sequence of servomotors for turning (with 4 steering segments as an example): steering segments are asynchronously actuated segments shown in Phase 0. The locomotion was gained with 2 × 2 peristaltic locomotion (Phase 1–6). (c) Turning radius depends on the number of steering segments. The effect of number of steering segments were experimentally investigated and results were plotted. Embedded images show top view of MetaCrawler. The scale bar represents a length of 50 cm.

diameter as large as possible provided faster speeds. Specifically, from the relationship between $\boldsymbol{\delta_y}$ and $\boldsymbol{D}$ show in figure 3(e), the fast peristalsis (0°–90°) occurred at diameters from about 12 cm to 10 cm. This 2 cm change in diameter was sufficient to lift contracted segments from the ground. As shown in figure 3(d), the model (equations (S1)–(S3)) can predict the trends in velocities that are coherent with the predictions by showing the same trend between selected servomotor rotation ranges. On the other hand, the accuracy of the predictions got higher in low speeds. We speculate that the ground friction influences motion at higher speeds. Because peristalsis is a locomotion mode that is primarily valuable in confined spaces, it may not always be possible to use the larger end of the segment diameter range. The robot can contract to as much as 60% of its maximum diameter (figure 3(e)). And even at the reduced diameter (e.g. within a 10 cm conduit), the robot still locomoted, albeit with lower speeds by decreasing the contracted segments (e.g. to 7 cm).

The unit cell behavior predicted overall robot speed until the weight of the contracted segments caused excessive deformation in the structure. We demonstrated this by increasing the number of contracted segments between anchoring segments for a single wave on the body (figure 3(f)). Ideally, because only the contracted segments are moving, increasing the number of contracted (moving) segments should increase the speed of the robot [33]. Experimentally, the speed increased from 2 to 4 segments in a wave, but when 5 segments were suspended between two maximum diameter segments (anchors), the speed decreases. This is because while a small number of contracted segments can be easily lifted off the ground, the increased weight of additional segments results in segments dragging along the ground, a trade-off discussed in our prior work [33]. Increasing the number of waves reduces the effect of friction by distributing the weight of contracted segments along the whole robot; therefore, using waveforms with higher number of waves results in higher speeds.

We also investigated the effect of cyclic loading on soft connectors' deformation behavior. Viscoelastic characteristics of TPU caused a compressive deformation resulting in ∼8% of a reduction in the vertical length of connectors that reached a steady state after 8% of the original span Y in the idle state after long use. On the other hand, this is not a plastic deformation; connectors recover after ∼30 min of relaxation time. This experiment confirms that the long use of the robot do not cause a permanent effect on the body structure. The reason why TPU as a lattice structure does not exhibit plastic behavior is that applied load resulting in flexure in connectors is significantly lower than previously reported loading conditions [49]. The details of the conducted experiment have been reported in the supplementary document.

5. Segment flexure: steering and undulatory locomotion modes

Steering and undulatory locomotion depend on the body's ability to bend [2, 50]. Segment flexure in MetaCrawler is generated via asynchronous actuation of the left and right servomotors. Contraction on one side of a segment causes larger elongation than the other, which bends the segment (figure 4(a)). Bending generated in MetaCrawler is measured as 15° per segment. We assessed the turning radius of the robot with different actuation sequences. We also investigated utilization of segment flexure for undulatory locomotion. We

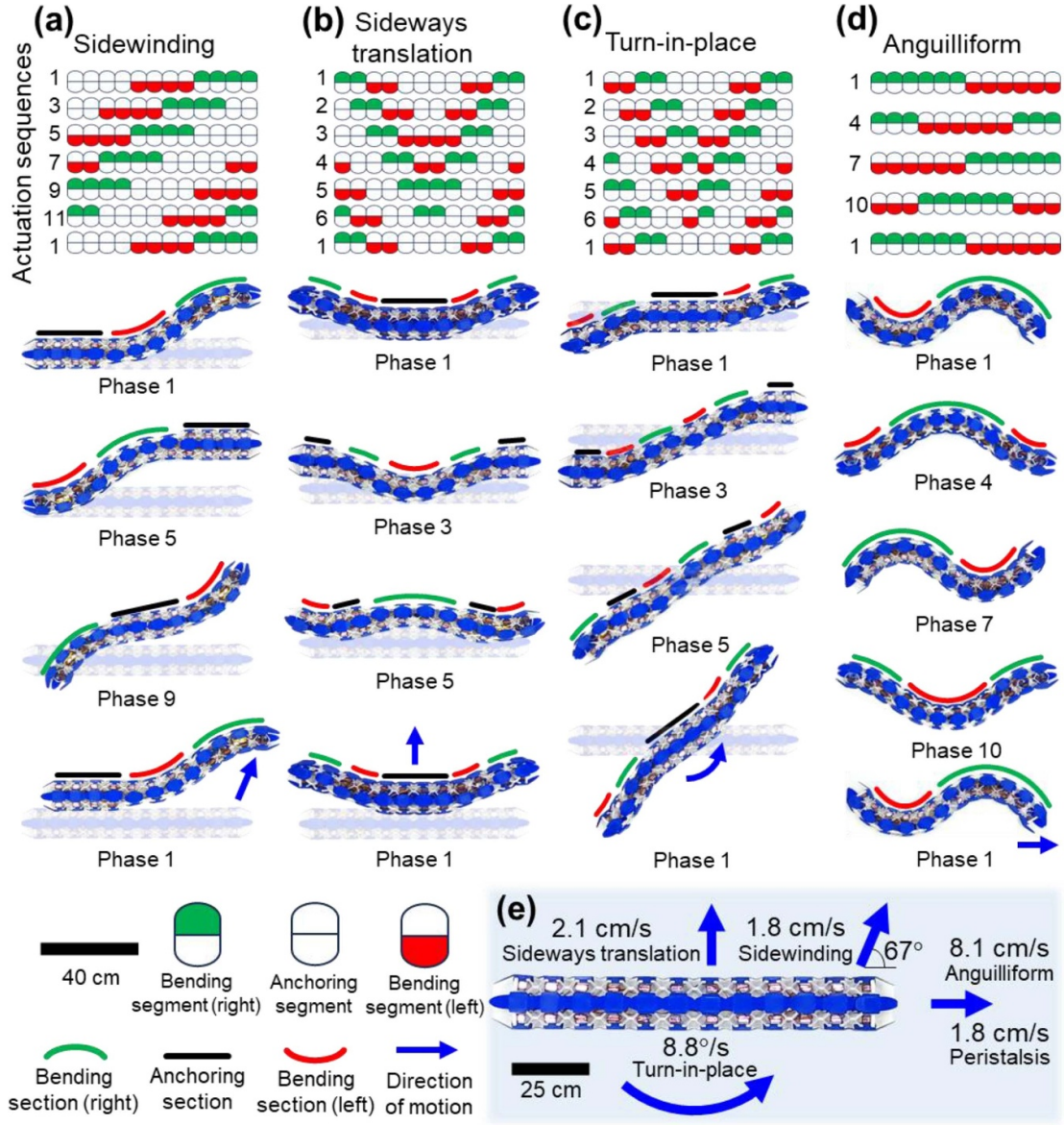

Figure 5. Undulatory locomotion gained by segment flexure-based actuation sequences. Images show top view of the robot. (a) MetaCrawler performs sidewinding with an actuation sequence forming a sine wave with the 4 right and 4 left bending segments propagating along the body. (b) Sideways translation is achieved with two symmetric sine waves with 2 right and 2 left bending segments propagating from the ends of the robot to the center. (c) Turn-in-place mode is programmed with two asymmetric sine waves with 2 right and 2 left bending segments propagating from the ends of the robot to the center. (d) Anguilliform locomotion is performed with a full-body undulation (6 right and 6 left segments). (e) Performing diverse locomotion modes, MetaCrawler exhibits an omnidirectional movement with presented velocities and directions.

then programmed MetaCrawler to perform various flexure-based waveforms generating sidewinding, anguilliform, sideways translation and turn-in-place (figure 5). Codes used for programming locomotion modes has been reported in the supplementary document.

5.1. Steering

First we demonstrated that segment flexure enables the robot to change direction. On smooth flat ground, MetaCrawler turned by bending the segments nearest the head of the robot while locomoting with peristalsis. For example, steering with the four front segments can be superimposed with 2×2 peristalsis, as shown in figure 4(b). The more segments were involved in steering, the tighter the turn became (as shown by a decrease in turning radius in figure 4(c)).

This is only one of many possible turning strategies that can be explored with this platform. For example, other robots have employed flexure-based traveling waves that use bending all along the body [51, 52]. Geometrically, it is sometimes possible to calculate actuation sequences which prevent anchoring segments from slipping [53]. These and many other combinations can be explored in

future work as needed, especially for soft or rough environments in which the robot cannot slide easily across the substrate.

5.2. Mode: sidewinding

A basic undulatory waveform is a traveling wave of four right bending, four left bending, and four anchoring segments. This results in diagonal locomotion as shown in figure 5(a) in which the body does not rotate, but translates such that when the cycle is complete the robot takes a position which is parallel to the previous position. We refer to this mode as 'sidewinding' because sidewinding snakes similarly move in a direction diagonal to the axis of their bodies [54]. Sidewinding gait was also demonstrated by others using orthogonal rotations to lift portions of the body off the ground, especially in soft sand [55]. On MetaCrawler, the expanded segments (anchors) have a larger diameter than the partially-contracted bent segments, reducing the surface contact on the ground to approximate this effect. MetaCrawler's sidewinding velocity is 1.8 mm s^{-1}. The angle between the axis of the body and the direction of movement is 67°.

5.3. Mode: sideways translation

In order to locomote in a perpendicular direction to the axis of the body, two symmetric small sidewinding waves (2 right and 2 left bending segments) start from the ends and move to the center of the robot. The locomotion starts with bending end segments to the movement direction (Phase 1) (figure 5(b)). While the undulation wave reaches central segments, end sections anchor to the ground (Phase 3). When the middle segments anchors, the robot pulls the central segments to the movement direction by bending this section in the opposite direction (Phase 5). Finally the central section anchors to the ground and the next cycle begins. The resulting velocity is 2.1 mm s^{-1}.

5.4. Mode: turn-in-place

Having the front and back halves of the robot perform sidewinding, but in opposite directions, rotates the robot in place about the normal axis to the ground passing the center of the mass of the robot [56]. Turn-in-place is performed with two asymmetric small sidewinding waves (2 right and 2 left bending segments) propagating from ends to the center of the body (figure 5(c)). The resultant angular velocity is 8.8° s^{-1}.

5.5. Mode: anguilliform locomotion

For swimming, we implemented an anguilliform waveform. Anguilliform locomotion is the mode of 2-dimensional undulatory swimming waves propagating posteriorly along the length of the animal, propelling it forward [3]. Anguilliform was attained by programming a full body undulation; a waveform that consists of 6 right and 6 left bending segments, forming sinusoidal curves (figure 5(d)). In order to test this capability, the robot was covered with a protective LDPE sleeve (supplementary document), and placed in a swimming pool. Anguilliform swimming was possible at a velocity of 8.1 mm s^{-1} with the robot floating on water (figure 6(a), supplementary movie S1).

6. Example uses of multimodal locomotion

We demonstrate various applications in different environments to show that the above mentioned modes can be easily combined to attain a range of locomotive behaviors. Actuation sequences used in referred supplementary movies were reported as figures in the supplementary document.

6.1. Confined channels

A retrieval of an object in a confined channel is an example of a potential use of MetaCrawler. As demonstrated in supplementary movie S2, MetaCrawler navigates in a channel which is ∼10% narrower than the expanded state of the body (figure 6(b)). The robot approaches the target, a mouse toy, with 2 × 1 waveform peristalsis. At the target, the contraction in the front segment is deactivated and peristalsis performed with the rest of the segments. When the head of the robot is in position, the front segment is contracted to secure the object and then held while the robot moves backward, carrying the object. Confined channels can also be traversed by MetaCrawler vertically against gravity, demonstrating the capability of the robot to traverse a pipe or conduit in any orientation (figure 6(c)). The radial stiffness of the metamaterial body anchored the MetaCrawler on the channel surface. Supplementary movie S3 demonstrates that MetaCrawler moves against gravity via peristalsis when placed in a vertically positioned transparent tubing. Small asymmetries in weight distribution and surface contact caused the robot to gradually rotate about the vertical axis but it did not impede the locomotion. In this demonstraion, the traction was increased by adhering rubber tapes (Scotch, 2228 Rubber Mastic Electrical Tape) on cover of the nodes. Other non-climbing applications of the MetaCrawler did not make use of rubber tapes because in our experience with CMMWorm, lower friction favors a faster locomotion [28].

Finally, we demonstrate that the combination of locomotion modes can be used to enter confined channels from open spaces, e.g. through a chamber with gates at the far corners (figure 6(d), supplementary movie S4). Each gait is an opening in the wall 30% narrower than expanded diameter. The robot locomotes with 2 × 3 peristalsis through the first gate and turns with 4 steering segments toward the second gate (as in figure 4(b)). The operator adjusts the robot's

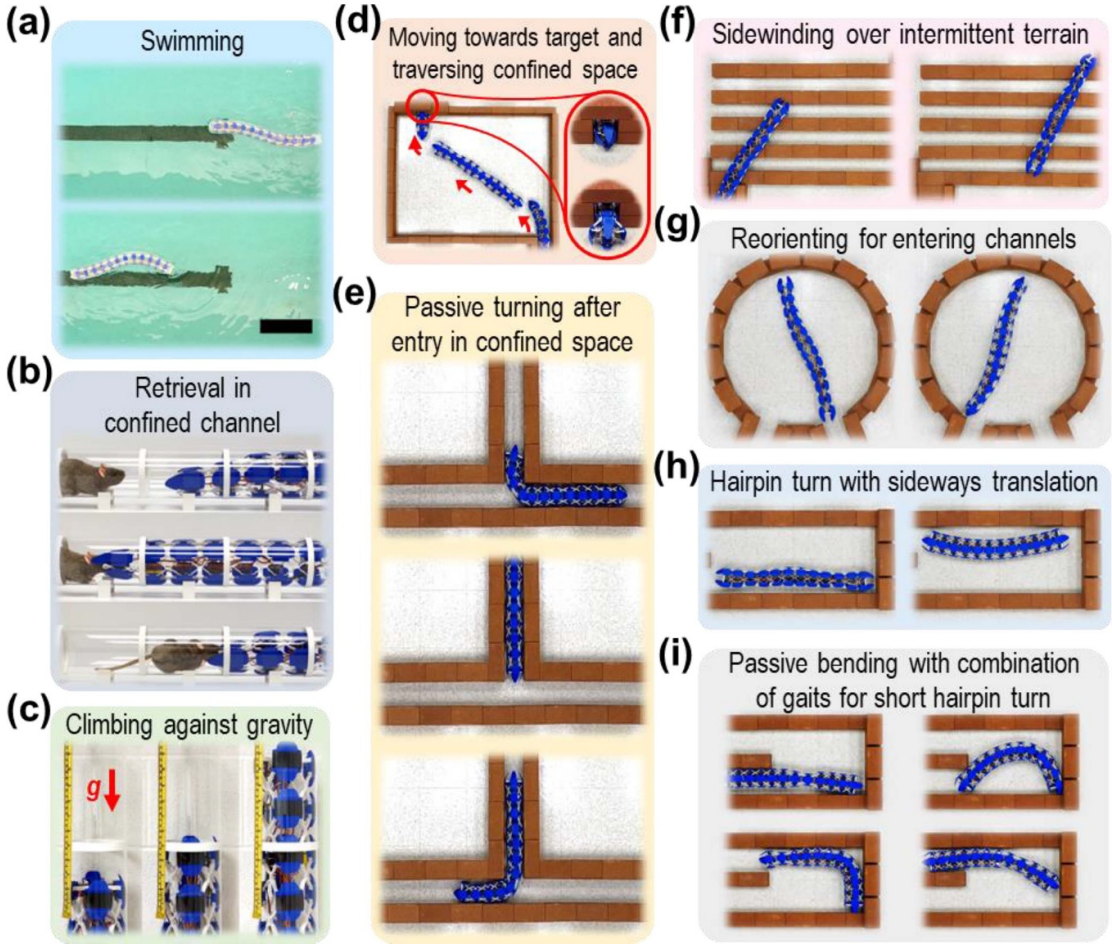

Figure 6. Examples uses of multimodal locomotion. MetaCrawler was tested to observe its performance in various environments and to demonstrate the significance of performing versatile locomotion. Videos from which the presented stills were taken are reported as supplementary movies. (a) Anguilliform swimming was tested in a pool. The robot was covered with a LDPE sleeve to secure electronics. The scale bar represents a length of 50 cm. (b) MetaCrawler traverses in confined channel with peristalsis and retrieve an object. In this application, one of the end segments was used as a gripper to carry an object. (c) Radial stiffness the nodal honeycomb segments enable the robot to climb up in a confined channel. To increase the friction, rubber tapes were added on node covers. Outer diameter of channels shown in (b) and (c) is 12 cm. (d) The robot enters in a chamber and move towards far corner via turning when required. It passes through the exit which is ∼30% narrower than the diameter of the robot. (e) T-mazes are challenging for limbless robots because of 90° turns. MetaCrawler can turn the head and tail in the desired direction to make the entry to the channel. After entry, the robot performs regular peristalsis to continue the gait without requiring additional turning actuation because the soft body structure passively turns itself. (f) Moving on intermittent terrains are difficult with peristaltic locomotion because the rectilinear motion requires the axis of the robot body to be close to the horizontal gaps which is a fall risk. Sidewinding enables continuous contact with the terrain without falling. (g) Turn-in-place is an efficient locomotion to reorient the robot to take position for entering channels. (h) Sideways translation enables the robot to move in the perpendicular direction of the body axis. This locomotion is efficient for hairpin turns. (i) When a hairpin turn is too short to perform sideways translation, custom actuation sequences can be programmed for to enable the robot to continue the gait. Actuation forces bend the compliant the body structure to take sharp turns in limited spaces to maneuver. Length of bricks shown in (d)–(i) is 20.3 cm.

direction until the tip enters the second gate. Then the robot locomotes with 2 × 3 peristalsis through the second gate. This demonstrates that unlike for a rigid, non-slipping robot little planning is required because the robot passively adapts.

6.2. Maze demonstrations

6.2.1. T-mazes

Within a maze, the robot can make even tighter turns than in open spaces because of passive bending of the soft body (figure 6(e), supplementary movie S5). This is important because infrastructure conduit networks often have 90° intersections. In the first example, the channel width is 20 cm and yet the turning mode in figure 4(b) is effective to access the side passage even though the unobstructed turning radius is much larger at 75 cm (figure 4(c)). The turning mode is only required at the beginning of the turn, and then the peristalsis mode is effective at carrying the robot through the turn due to passive compliance. The robot also can back-up and continue moving in the original direction. In narrower channels (12 cm), the same process takes additional time (an additional 60%) and more precise control. The strategy we found effective was keeping the front steering segments bent while peristaltically

locomoting with remaining segments (1:10–1:15 of supplementary movie S5). Then the robot can use peristalsis to slide the rest of the body past the sharp 90° corner (1:15–1:56).

6.2.2. Intermittent terrain

Terrains with intermittent support (e.g. rough surfaces, floor grates, traction features, gaps between platforms) can cause a robot to fall or get stuck. Here we show that the robot can use a combination of peristalsis and sidewinding to traverse gaps that are close to the diameter of the robot (supplementary movie S6, figure 6(f)). Peristalsis (2×3) is effective to move perpendicular to the gaps and sidewinding enables motion parallel to the gaps. Note that the operator adjusts the position to keep the robot on the terrain.

6.2.3. Reorienting for entering channels

Not all channels intersect at right angles, the turn-in-place mode can save time adjusting the position of the body if, for example, multiple channels lead into a larger chamber, as we show in figure 6(g) and supplementary movie S7.

6.2.4. Hairpin turns

Finally, we wanted to show passive bending in the sharpest possible turns in which the channel changes direction 180° (a.k.a. a hairpin turn). If there is room for the tail to clear the wall that separates the two directions, the robot can simply switch from a peristaltic mode to the sideways translation mode and back (figure 6(h), supplementary movie S8). However, even in a shorter hairpin turn, in which there is only half the length of the prior example, MetaCrawler can passively fold to make a turn (figure 6(i), supplementary movie S9). The bend is initiated by steering into a corner with peristalsis. Then an undulatory mode with 2 right and 2 left bending segments quickly folds the front of the robot against the back wall until the tail is clear of the separating wall. Then the tail of the robot leads peristaltic locomotion, and the body straightens as it exits.

7. Discussions and conclusions

In this study, we built a soft robot body structure through 3D printing and discrete assembly [46] of modular nodal honeycomb [47] in a tubular form which combines hard nodes and soft connectors (figure 1). Soft connectors provided compliance to the structure while hard nodes enable on-board integration of servomotors, batteries and control circuitry (figure 2). We have shown the mechanical behaviour of nodal honeycomb unit cells and how their deformation profile is utilized to estimate the speed and passable dimensions of confined spaces with peristalsis (figure 3). We also demonstrated turning and undulatory locomotion modes resulted from various flexure-based actuation sequences (figures 4 and 5). Finally, we demonstrated the utility of multimodal locomotion in addressing potential challenges (figure 6).

An important aspect of this study lies in employing a lattice structure as a soft robot body, offering a simple design and fabrication process despite its sophisticated functionality. The modular design strategy enabled an easy fabrication process which can be performed by any 3D printer. Press-fit-based discrete assembly of 3D printed nodes and connectors minimized manual labor. Therefore, this concept offers scalability for different applications and customizability for different objective functions. On the other hand, the design is dependent on the size of servomotors. This concept can be scaled down for smaller servomotors but it cannot be further miniaturized for applications like gastrointestinal robots.

The ease of fabrication also faciliated the addition of segments to the robot more easily than previous designs, enabling the investigation of multimodal locomotion. Table S1 presents comparable previous soft robots with their actuation systems, locomotion modes and segment lengths. This comparison demonstrates how locomotion versatility is related to the number of segments and segment length. The segment length of MetaCrawler is 34% shorter than the closest counterpart which provides a better control in body position and enable performing more locomotion modes (table S1).

Having short segment length in limbless robots is important for efficient locomotion. Importance of segment length is especially realized in steering and undulatory locomotion. For example, compared to our previous design, CMMWorm-S [53], MetaCrawler generates 35% higher bending per segment. On the other hand, when the bending is calculated per unit length, MetaCrawler generates 2.5 times higher bending because the segment length in MetaCrawler is 40% shorter than CMMWorm-S. (table S1).

A major advantage of the nodal honeycomb is accommodating the entire actuation system onboard. Our approach enabled integrating commonly used hard robotic tools in a compliant body structure. Utilization of servomotors, control circuits, and batteries both simlified programming locomotion modes and learning the operation of the robot.

The analytical model predicted the trends in experimental velocities faithfully for different peristalsis patterns under varying servomotor rotation ranges. However, there were discrepancies between the model and the experiments at higher speeds

which we speculate to result from friction effects that the model does not account for. Integrating friction as a parameter in a mathematical model characterizing the speed of the robot requires considering the magnitude of deflection in contracted segments caused by the gravity. Although this can be determined with a finite element analysis, the complexity of the lattice geometry makes the mathematical modeling significantly challenging.

The actuation system in this design applies dynamic loading on soft connectors and tendons, which may raise concerns for long-term use. Our investigation confirms that the viscoelastic property of TPU causes a compressive deformation after prolonged use. Although this is not a permanent plastic deformation and the connectors recover over time after operations cease, this may affect the speed because the connectors cannot regain their original expansion state during locomotion. This issue can be eliminated by using materials which are resistant to viscoelastic effects; however, the current state of commercial soft filaments cannot offer an alternative for TPU. On the other hand, the tendons, which experience cyclic tension, do not exhibit significant deformation. Another concern may arise from damage due to the friction that occurs between the nodes and tendons. Despite the fact that no damage was observed in the nodes and tendons, this concern could be mitigated by placing PTFE tubing at the tendon entry holes on the side nodes. Considering that this concept is compatible with scaling up, lubrication may be necessary for larger versions of MetaCrawler.

The major limitation in our demonstrations is that they are all limited to planar motion. Although the segment contraction enables the robot to raise the structure from the ground, it is not sufficient to climb over obstacles. Three-dimensional movement can be addressed with addition of actuators on top and bottom nodes, and modification in the nodal honeycomb structure to satisfy structural stiffness requirements in future versions of the robot. On the other hand, even the current prototype can be helpful for certain usage. For example, as supplementary movie S2 shows, the robot can be used to retrieve objects by utilizing segment contraction as a gripper. This ability can be useful for pipeline or sewer maintenance. Especially a network of lines where branching of pipes, or diametral variations in transition points would be suitable for MetaCrawler. Similarly, the robot can carry lightweight objects efficiently which can be used to transport medication to victims in disaster zones.

The next stage of this research includes testing the MetaCrawler in real-world environments. Unpredictability of unstructured environments requires the robot to have versatility in locomotion. Although the demonstrations in supplementary movies are not unstructured environments, they exhibit certain challenges which the robot must overcome to continue its travel. Unstructured environments, for example wreckages after earthquakes, combine multiple challenges in the same mission. Therefore, the ability that MetaCrawler demonstrates in especially supplementary movies S3, 5 and 9 will be extremely useful. Similarly, military surveillance and reconnaissance missions may require travels on both ground and water. Therefore, having both terrestrial and aquatic locomotions will be helpful to complete tracks.

Another improvement which needs to be done is securing electronics from environmental damaging factors such as dust, soil, mud, etc. Although we integrated a sleeve on robot's body for the swimming tests, we observed that it is not compatible for on-ground locomotion. The research will continue to develop a skin for the robot which does not affect the locomotion.

The robot demonstrated both multimodal and omnidirectional locomotion. Bioinspired peristalsis, sidewinding, anguilliform locomotion as well as derivate sideways translation and turn-in-place were implemented by programming the robot with specific actuation sequences of servomotors. Although, previous studies have reported hard robots with multimodal undulatory locomotion modes [57], current study presents a robust alternative with structural compliance as well as easy fabrcation.

As being the first metamaterial-based, untethered soft bodied system with multimodal locomotion, MetaCrawler is an important improvement in limbless soft robots. Its features make it suitable for various applications, including search and rescue operations, pipeline inspection, undersea explorations, and space missions. As we look to the future, potential enhancements include integrating more motors for 3D locomotion, utilizing continuous servomotors for larger segment contraction ranges, and sensor integration. The ease of use and the broad range of potential applications position MetaCrawler as a promising innovation with translational potential in the soft robotics.

Data availability statement

The data that support the findings of this study are available upon reasonable request from the authors.

Acknowledgments

This research was supported by a fellowship from the Republic of Türkiye Ministry of National Education (YD), and the Kent Hale Smith Endowment (OA). The authors would like to acknowledge Dr. Melinda Lake-Speers for providing space for experiments; Mr. Huseyin Aydogmus for his assistance in preliminary circuit design; Ms. Seniye Sertel for her support in

locomotion analyses; and Mr. Nazım Dikici for the fabrication of the sleeve used for swimming tests.

ORCID iDs

Yusuf Dikici https://orcid.org/0000-0002-7061-2550
Kathryn Daltorio https://orcid.org/0000-0001-6994-1536
Ozan Akkus https://orcid.org/0000-0003-3523-3421

References

[1] Juhász Z and Zelei A 2013 Analysis of worm-like locomotion *Period. Polytech. Mech. Eng.* **57** 59–64
[2] Jayne B C 2020 What defines different modes of snake locomotion? *Integr. Comp. Biol.* **60** 156–70
[3] Gillis G B 1996 Undulatory locomotion in elongate aquatic vertebrates: anguilliform swimming since Sir James Gray[1] *Am. Zool.* **36** 656–65
[4] Li G, Zhang H and Zhang J 2023 *Bio-Inspired Locomotion Control of Limbless Robots* (Springer)
[5] Trivedi D, Rahn C D, Kier W M and Walker I D 2008 Soft robotics: biological inspiration, state of the art, and future research *Appl. Bionics Biomech.* **5** 99–117
[6] Zhao W, Zhang Y and Wang N 2021 Soft robotics: research, challenges, and prospects *JRM* **33** 45–68
[7] El-Atab N, Mishra R B, Al-Modaf F, Joharji L, Alsharif A A, Alamoudi H, Diaz M, Qaiser N and Hussain M M 2020 Soft actuators for soft robotic applications: a review *Adv. Intell. Syst.* **2** 2000128
[8] Li M, Pal A, Aghakhani A, Pena-Francesch A and Sitti M 2022 Soft actuators for real-world applications *Nat. Rev. Mater.* **7** 235–49
[9] Rich S I, Wood R J and Majidi C 2018 Untethered soft robotics *Nat. Electron.* **1** 102–12
[10] Tolley M T, Shepherd R F, Mosadegh B, Galloway K C, Wehner M, Karpelson M, Wood R J and Whitesides G M 2014 A resilient, untethered soft robot *Soft Robot.* **1** 213–23
[11] Onal C D and Rus D 2013 Autonomous undulatory serpentine locomotion utilizing body dynamics of a fluidic soft robot *Bioinsp. Biomim.* **8** 026003
[12] Chubb K, Berry D and Burke T 2019 Towards an ontology for soft robots: what is soft? *Bioinsp. Biomim.* **14** 063001
[13] Ozkan-Aydin Y, Liu B, Ferrero A C, Seidel M, Hammond F L and Goldman D I 2021 Lateral bending and buckling aids biological and robotic earthworm anchoring and locomotion *Bioinsp. Biomim.* **17** 016001
[14] Li P, Chen B and Liu J 2023 Multimodal steerable earthworm-inspired soft robot based on vacuum and positive pressure powered pneumatic actuators *Bioinsp. Biomim.* **19** 016001
[15] Tang Z, Lu J, Wang Z, Ma G, Chen W and Feng H 2020 Development of a new multi-cavity pneumatic-driven earthworm-like soft robot *Robotica* **38** 2290–304
[16] Tang Z, Lu J, Wang Z, Chen W and Feng H 2020 Design of a new air pressure perception multi-cavity pneumatic-driven earthworm-like soft robot *Auton. Robots* **44** 267–79
[17] Zhou X, Teng Y and Li X 2016 Development of a new pneumatic-driven earthworm-like soft robot *2016 23rd Int. Conf. on Mechatronics and Machine Vision in Practice (M2VIP)* pp 1–5
[18] Seok S, Onal C D, Cho K-J, Wood R J, Rus D and Kim S 2013 Meshworm: A peristaltic soft robot with antagonistic nickel titanium coil actuators *IEEE/ASME Trans. Mechatronics* **18** 1485–97
[19] Niiyama R, Matsushita K, Ikeda M, Or K and Kuniyoshi Y 2022 A 3D printed hydrostatic skeleton for an earthworm-inspired soft burrowing robot *Soft Matter* **18** 7990–7
[20] Muff L F, Mills A S, Riddle S, Buclin V, Roulin A, Chiel H J, Quinn R D, Weder C and Daltorio K A 2023 Modular design of a polymer-bilayer-based mechanically compliant worm-like robot *Adv. Mater.* **35** 2210409
[21] Wan Z, Sun Y, Qin Y, Skorina E H, Gasoto R, Luo M, Fu J and Onal C D 2023 Design, analysis, and real-time simulation of a 3D soft robotic snake *Soft Robot.* **10** 258–68
[22] Bi Z, Zhou Q and Fang H 2023 A worm-snake-inspired metameric robot for multi-modal locomotion: design, modeling, and unified gait control *Int. J. Mech. Sci.* **254** 108436
[23] Qin Y, Wan Z, Sun Y, Skorina E H, Luo M and Onal C D 2018 Design, fabrication and experimental analysis of a 3D soft robotic snake *2018 IEEE Int. Conf. on Soft Robotics (Robosoft)* pp 77–82
[24] Andersen K B, Kandhari A, Chiel H J, Quinn R D and Daltorio K A 2018 A nitinol-actuated worm robot bends for turning and climbing obstacles *Biomimetic and Biohybrid Systems Lecture Notes in Computer Science* ed V Vouloutsi, J Halloy, A Mura, M Mangan, N Lepora, T J Prescott and P F M J Verschure (Springer) pp 6–10
[25] Horchler A D *et al* 2015 Worm-like robotic locomotion with a compliant modular mesh *Biomimetic and Biohybrid Systems Lecture Notes in Computer Science* ed S P Wilson, P F M J Verschure, A Mura and T J Prescott (Springer) pp 26–37
[26] Lee H, Jang Y, Choe J K, Lee S, Song H, Lee J P, Lone N and Kim J 2020 3D-printed programmable tensegrity for soft robotics *Sci. Robot.* **5** eaay9024
[27] Parra Rubio A, Fan D, Jenett B, Del Águila Ferrandis J, Tourlomousis F, Abdel-Rahman A, Preiss D, Zemánek J, Triantafyllou M and Gershenfeld N 2023 Modular morphing lattices for large-scale underwater continuum robotic structures *Soft Robot.* **10** 724–36
[28] Horchler A D *et al* 2015 Peristaltic locomotion of a modular mesh-based worm robot: precision, compliance, and friction *Soft Robot.* **2** 135–45
[29] Kandhari A, Huang Y, Daltorio K A, Chiel H J and Quinn R D 2018 Body stiffness in orthogonal directions oppositely affects worm-like robot turning and straight-line locomotion *Bioinsp. Biomim.* **13** 026003
[30] Kandhari A, Mehringer A, Chiel H J, Quinn R D and Daltorio K A 2019 Design and actuation of a fabric-based worm-like robot *Biomimetics* **4** 13
[31] Kandhari A, Stover M C, Jayachandran P R, Rollins A, Chiel H J, Quinn R D and Daltorio K A 2018 Distributed sensing for soft worm robot reduces slip for locomotion in confined environments *Biomimetic and Biohybrid Systems Lecture Notes in Computer Science* eds V Vouloutsi, J Halloy, A Mura, M Mangan, N Lepora, T J Prescott and P F M J Verschure (Springer) pp 236–48
[32] Huang Y, Kandhari A, Chiel H J, Quinn R D and Daltorio K A 2017 Slip reduction controls of mesh-body worm robot developed from a mathematical model *2017 IEEE Int. Conf. on Robotics and Biomimetics (ROBIO)* pp 1474–9
[33] Kandhari A, Wang Y, Chiel H J, Quinn R D and Daltorio K A 2021 An analysis of peristaltic locomotion for maximizing velocity or minimizing cost of transport of earthworm-like robots *Soft Robot.* **8** 485–505
[34] Craster R, Guenneau S, Kadic M and Wegener M 2023 Mechanical metamaterials *Rep. Prog. Phys.* **86** 094501
[35] Jiao P, Mueller J, Raney J R, Zheng X and Alavi A H 2023 Mechanical metamaterials and beyond *Nat. Commun.* **14** 6004
[36] Yu X, Zhou J, Liang H, Jiang Z and Wu L 2018 Mechanical metamaterials associated with stiffness, rigidity and compressibility: a brief review *Prog. Mater. Sci.* **94** 114–73
[37] Li T, Hu X, Chen Y and Wang L 2017 Harnessing out-of-plane deformation to design 3D architected lattice metamaterials with tunable Poisson's ratio *Sci. Rep.* **7** 8949

[38] Jia Z, Liu F, Jiang X and Wang L 2020 Engineering lattice metamaterials for extreme property, programmability, and multifunctionality *J. Appl. Phys.* **127** 150901
[39] Fang H, Zhang Y and Wang K W 2017 Origami-based earthworm-like locomotion robots *Bioinsp. Biomim.* **12** 065003
[40] Li D *et al* 2023 Origami-inspired soft twisting actuator *Soft Robot.* **10** 395–409
[41] Rafsanjani A, Zhang Y, Liu B, Rubinstein S M and Bertoldi K 2018 Kirigami skins make a simple soft actuator crawl *Sci. Robot.* **3** eaar7555
[42] Branyan C, Rafsanjani A, Bertoldi K, Hatton R L and Mengüç Y 2022 Curvilinear kirigami skins let soft bending actuators slither faster *Front. Robot. AI.* **9** 872007
[43] Ren X, Das R, Tran P, Ngo T D and Xie Y M 2018 Auxetic metamaterials and structures: a review *Smart Mater. Struct.* **27** 023001
[44] Miura K 1985 Method of packaging and deployment of large membranes in space *Inst. Space Astronaut. Sci. Rep.* **1** 618
[45] Imre A 2014 Metamaterials with negative compressibility—a novel concept with a long history *Mater. Sci.* **32** 126–9
[46] Jenett B, Cameron C, Tourlomousis F, Rubio A P, Ochalek M and Gershenfeld N 2020 Discretely assembled mechanical metamaterials *Sci. Adv.* **6** eabc9943
[47] Dikici Y, Jiang H, Li B, Daltorio K A and Akkus O 2022 Piece-by-piece shape-morphing: engineering compatible auxetic and non-auxetic lattices to improve soft robot performance in confined spaces *Adv. Eng. Mater.* **24** 2101620
[48] Kanu E N, Daltorio K A, Quinn R D and Chiel H J 2015 Correlating kinetics and kinematics of earthworm peristaltic locomotion *Biomimetic and Biohybrid Systems (Lecture Notes in Computer Science)* ed S P Wilson, P F M J Verschure, A Mura and T J Prescott (Springer) pp 92–96
[49] Wang S, Tang S, He C and Wang Q 2023 Cyclic deformation and fatigue failure mechanisms of thermoplastic polyurethane in high cycle fatigue *Polymers* **15** 899
[50] Ma S 1999 Analysis of snake movement forms for realization of snake-like robots *Proc. 1999 IEEE Int. Conf. on Robotics and Automation (Cat. No.99CH36288C)* vol 4 pp 3007–13
[51] Omori H, Nakamura T and Yada T 2009 An underground explorer robot based on peristaltic crawling of earthworms *Ind. Robot.* **36** 358–64
[52] Omori H, Hayakawa T and Nakamura T 2008 Locomotion and turning patterns of a peristaltic crawling earthworm robot composed of flexible units *2008 IEEE/RSJ Int. Conf. on Intelligent Robots and Systems* (IEEE) pp 1630–5
[53] Kandhari A, Wang Y, Chiel H J and Daltorio K A 2019 Turning in worm-like robots: the geometry of slip elimination suggests nonperiodic waves *Soft Robot.* **6** 560–77
[54] Tingle J L, Sherman B M and Garland T Jr 2022 Scaling and relations of morphology with locomotor kinematics in the sidewinder rattlesnake Crotalus cerastes *J. Exp. Biol.* **225** jeb243817
[55] Marvi H, Gong C, Gravish N, Astley H, Travers M, Hatton R L, Mendelson J R, Choset H, Hu D L and Goldman D I 2014 Sidewinding with minimal slip: snake and robot ascent of sandy slopes *Science* **346** 224–9
[56] Tesch M, Lipkin K, Brown I, Hatton R, Peck A, Rembisz J and Choset H 2009 Parameterized and scripted gaits for modular snake robots *Adv. Robot.* **23** 1131–58
[57] Hatton R L, Knepper R A, Choset H, Rollinson D, Gong C and Galceran E 2013 Snakes on a plan: toward combining planning and control *2013 IEEE Int. Conf. on Robotics and Automation* pp 5174–81